J Intell Robot Syst
DOI 10.1007/s10846-013-9871-1

Control of a Mobile Robot Subject to Wheel Slip

Yu Tian · Nilanjan Sarkar

Received: 24 December 2011 / Accepted: 25 July 2013

Abstract Wheel slip is inevitable when a Wheeled Mobile Robot (WMR) is moving at a high speed or on a slippery surface. In particular, when neither lateral nor longitudinal slips can be ignored in the dynamic model, a WMR becomes an underactuated nonlinear dynamic system. To study the maneuverability of a WMR in such a realistic environment, we model the overall WMR dynamics subject to wheel slip and propose control algorithms in regulation control and turning control tasks for the WMR. In regulation control, a time-invariant discontinuous feedback law is developed to asymptotically stabilize the system to the desired configuration with exponential convergence rate. In turning control, a sliding mode-based extremum seeking control technique is applied to achieve stable and sharp turning. Simulation results are presented to validate the theoretical results.

Keywords Wheeled mobile robot · Wheel slip · Extremum seeking control · Traction force · Underactuated system

Y. Tian (✉) · N. Sarkar
Department of Mechanical Engineering,
Vanderbilt University, Nashville, TN, USA
e-mail: ytian.xp@gmail.com

N. Sarkar
e-mail: nilanjan.sarkar@vanderbilt.edu

1 Introduction

As nonholonomic WMRs have been increasingly applied to high-speed operation in unstructured environment, wheel slip becomes an issue when ideal rolling assumption is not satisfied. In an ideal rolling constraint, the wheels of a mobile robot are assumed to roll without slipping. This ideal rolling constraint may be violated when the robot is either accelerating, or decelerating, or turning at a high speed. Ignoring the effect of wheel slip may cause several problems—the mobile robot may deviate from a desired path and thereby not complete a mission, and sometimes a stable system may even become unstable.

There are a few recent papers that present approaches to modeling wheel slips in both WMR community and vehicle engineering community. In WMR community, [1] is one of the earliest works that considers slip in the WMR dynamic model. The authors considered small values of slip ratios on which traction force was linearly dependent. They then developed a slow manifold approach to design output feedback control law. In [2] anti-slip factor was introduced to represent the percentage of a wheel's angular speed that reflects the wheel's forward speed. This same factor also represents the percentage of the wheel's driving force reflected effectively by the road friction. The road friction was considered as unmodeled dynamics. Neural network technique was

Published online: 09 August 2013

applied to realize optimal speed tracking control. In [3] slip states were introduced into a generalized WMR kinematic model. In [4] slip was considered as a small, measurable, bounded disturbance in the WMR kinematic model, and a kinematic control law was developed to overcome the disturbance. In [5] wheel slip was considered uncertainty in robot dynamics and a robust control was designed to suppress it. In [6] skid-slip effect for a WMR was considered as disturbance on kinematic model, estimated using Kalman filter and compensated in a position tracking control. In [7] longitudinal traction force was included in an omni-directional WMR model by externally measuring the magnitude of slip. However, the ideal WMR model was used in control design for simplicity. In [8] lateral traction force was introduced that was linearly dependent on lateral slip, and a steering control approach was applied to lateral position tracking control for a bicycle model. In [9] longitudinal slip dynamics was considered in an omni-directional WMR model. However in the control law derivation, pure rolling was assumed to obtain a relationship between the driving torque and the traction force. In [10] both longitudinal and lateral tractions were introduced, which were approximated to be linearly dependent on longitudinal and lateral slip, respectively, for a reduced unicycle model representing a four-wheel-drive WMR. In the controller design, slips and steering torque were control inputs to be designed first, and then by assuming that tire dynamics was significantly faster than the WMR dynamics, driving torque was designed to control the vehicle. As can be seen from the above literature survey, researchers have made significant contributions in modeling and control of mobile robots with wheel slip. Our current work builds on this research to develop a new control strategy for the regulation control and sharp turning control of a WMR subject to wheel slip. In vehicle engineering community, however, traction forces are modeled rigorously for four-wheel vehicle systems. But, in general, these works do not consider nonholonomic constraint equations in their model of the vehicle dynamics as can be seen in [11–14]. This is mainly because position control is not a main concern in vehicle control and they focus more on engine, drive train and transmission dynamics and control than the vehicle body dynamics. However, in this paper, we are mostly interested in the WMR body dynamics and control in applications where position control is a main concern. Note that, wheel slip is integrally related to traction force and thus a thorough analysis of control of a WMR with wheel slip requires the development of a dynamic model of the WMR to incorporate traction forces.

In our previous work [33], we modeled the WMR dynamics subject to wheel slip, where we incorporated slip-traction characteristic into the wheel dynamics. There is no actuation in the lateral direction of a WMR. The lateral traction force has to be controlled indirectly by the wheel torques. In [33] we applied sliding mode-based extremum seeking control [16] technique to design a control law to maximize the lateral traction force so that the turning radius during motion was minimized. We then used such a WMR as the pursuer in a Pursuit–Evasion game problem. Such a pursuer has a better chance to win the game given the capability of taking sharp turns by maximizing its lateral traction force.

In this paper, we further advanced the control of the WMR in the presence of slip. In particular, we proposed a new technique for configuration control of the WMR. Traditional control approaches for an ideal WMR dynamic model using time-invariant continuous feedback cannot control such a system to an equilibrium solution [15]. In this work, in order to achieve position control, we have modeled the overall WMR as a third order under-actuated dynamic system with a second order nonholonomic constraint. Such a model is different from a typical ideal WMR dynamic model in the sense that the second order nonholonomic constraint does not reduce the dimension of the state space. Motivated by the surface vessel control methodology [15], our contribution is to design and apply a time-invariant discontinuous feedback control law to asymptotically stabilize the WMR model to a desired configuration. *To the best of our knowledge, this is the first work in the literature that develops a regulation control mechanism for a WMR that is under-actuated due to wheel slip.* We believe that these new set of controllers will allow a WMR to move faster and in a

stable but dexterous manner when the terrain is slippery.

This paper is organized as follows. In Section 2 the dynamic model of a WMR subject to wheel slip is presented. In Section 3, control laws are designed for the WMR to achieve regulation control and sharp turning control. In Section 4 we validate the control laws via simulations. We then conclude the paper in Section 5.

2 Dynamic Model of a WMR Subject to Wheelslip

In this paper, the WMR subject to wheel slip is modeled as in Fig. 1, where Pc is the center of mass of the WMR, P_0 is the center of the wheel shaft, d is the distance from Pc to P_0, b is the distance from the center of each wheel to P_0. F_1 and F_2 are the longitudinal traction forces for $wheel_1$ and $wheel_2$, respectively. F_3 is the lateral traction force. To take the slip effect into account, dynamic model needs to be studied instead of kinematic model. The equations for the dynamic WMR model derived based on Newton's Law are shown in Eqs. 1.

$$\begin{cases} m\ddot{x}_c = (F_1 + F_2)\cos\varphi - F_3 \sin\varphi \\ m\ddot{y}_c = (F_1 + F_2)\sin\varphi + F_3 \cos\varphi \\ I\ddot{\varphi} = (F_1 - F_2)b - F_3 d \end{cases} \tag{1a}$$

$$\begin{cases} I_w\ddot{\theta}_1 = \tau_1 - F_1 r \\ I_w\ddot{\theta}_2 = \tau_2 - F_2 r \end{cases} \tag{1b}$$

where m is the robot mass, I is its moment of inertia, I_w is the moment of inertia of each wheel about the wheel axis, r is the wheel radius, φ is the orientation of the WMR, θ_i is the angular displacement of the i-th wheel, τ_i is the wheel torque applied to the i-th wheel. Equation 1a represents the entire WMR dynamics in the plane motion while Eq. 1b represents the spinning dynamics of the wheels.

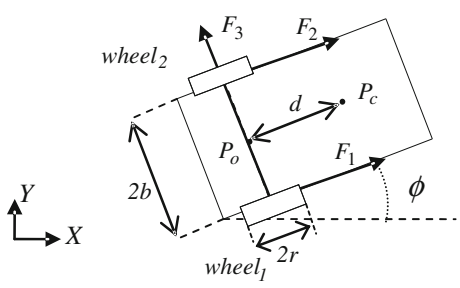

Fig. 1 WMR model subject to wheel slip

Slip is modeled as slip angle (sa) and slip ratio (sr),

$$sr_i = \frac{r\dot{\theta}_i - v_i}{v_i}, \quad sa = \tan^{-1}\left(\frac{\dot{\eta}}{v}\right) \tag{2}$$

where v_i is the longitudinal speed of the center of the i-th wheel, $v = (v_1 + v_2)/2$ is the forward speed, $\dot{\eta}$ is the lateral speed of the center of each wheel. They satisfy the following nonholonomic constraints [17]

$$v_1 = \dot{x}_c \cos\varphi + \dot{y}_c \sin\varphi + b\dot{\varphi} \tag{3}$$

$$v_2 = \dot{x}_c \cos\varphi + \dot{y}_c \sin\varphi - b\dot{\varphi} \tag{4}$$

$$\dot{\eta} = \dot{y}_c \cos\varphi - \dot{x}_c \sin\varphi - d\dot{\varphi} \tag{5}$$

Note that, unlike classical nonholonomic constraints of WMR, the above constraints allow both longitudinal and lateral slips.

In order to model the slip, traction forces and to design controllers, we need to have the knowledge of slip and dependency of traction forces on slip.

Usually the analytical dependency of traction forces on slip is difficult to formulate due to wheel temperature, thread pattern, camber angle and so on. However, the general behaviors of this dependency for rubber tire have been reported in [21]. In [22] an excellent review of current trends in modeling traction forces is provided using different methods, e.g., empirical, semi-empirical and analytical methods. Specifically, piecewise linear model, Buckhardt model, Rill model, Dahl model, Lugre model and Pacejka model or known as the Magic Formula are discussed therein.

The Magic formula model is an elegant, semi-empirical model based on curve fitting. It has been widely accepted in industry and academia to generalize the model of both longitudinal and lateral traction forces. It was introduced in [23]

and has been revised several times since then. This model has the advantage of accuracy, simplicity and ability to be interpreted over other models. Due to this reason, we employ the Magic Formula to model traction forces. In this model, the lateral and the longitudinal traction forces are functions of slip angle and slip ratio as

$$F = K_1 \sin\left(K_2 \tan^{-1}\left(SK_3 + K_4\left(\tan^{-1}\left(SK_3\right) - SK_3\right)\right)\right) + S_v \tag{6}$$

where S is a function of slip angle for the lateral traction force or slip ratio for the longitudinal traction force. All other variables K_i, $i = 1, \ldots, 4$ and S_v are constants and are determined from the curve fitting process of the empirical data. K_1 is proportional to friction coefficient. Figure 2a shows an example of lateral traction forces with friction coefficient 0.7 and 0.3, respectively. Figure 2b shows an example of longitudinal traction forces with friction coefficient 0.7 and 0.3, respectively.

Since $F_i(i=1,2)$ is a functions of $sr_i(i=1,2)$, $sr_i(i=1,2)$ is a function of $\dot{\theta}_i(i=1,2)$ and $\ddot{\theta}_i(i=1,2)$ is a function of $\tau_i(i=1,2)$, $\dot{F}_i(i=1,2)$ becomes a function of $\tau_i(i=1,2)$, as shown in Eq. 7. Thus after taking a derivative of Eq. 1a, it becomes a third order system with τ_i as the input. Note that since F_1 and F_2 are the only control inputs to Eq. 1a, Eq. 1a becomes an underactuated system with a second order nonholonomic constraint.

$$\dot{F}_i = \frac{K_1 K_2 \cos\left(K_2 \tan^{-1}\left(K_3 sr_i + K_4\left(\tan^{-1}(K_3 sr_i) - K_3 sr_i\right)\right)\right)\left(K_3 + K_4\left(\frac{K_3}{1+K_3^2 sr_i^2} - K_3\right)\right)}{1+(K_3 sr_i + K_4(\tan^{-1}(K_3 sr_i) - K_3 sr_i))^2} \frac{r v_i \tau_i - F_i r^2 v_i - r I_w \dot{\theta}_i \dot{v}_i}{I_w v_i^2} \tag{7}$$

Note that, this model assumes that slip can be measured. Measurement of wheel slip has been an active research area and researchers have used different combinations of sensors and estimation techniques to measure the slip. For example, in [18] Kalman filter was adopted to estimate the slip using the data collected from wheel encoder, global positioning system (GPS) and inertial measuring unit (IMU). In [19] the amount of slip of an exploration rover was predicted by comparing current visual information with previous experience. In [20] a purely proprioceptive navigation strategy was presented using gyro, accelerometers and wheel encoders. The states (i.e., slip accelerations) were estimated using the extended Kalman filter. We do not present a survey of such techniques in this paper—we assume that slip information will be available to develop our controllers.

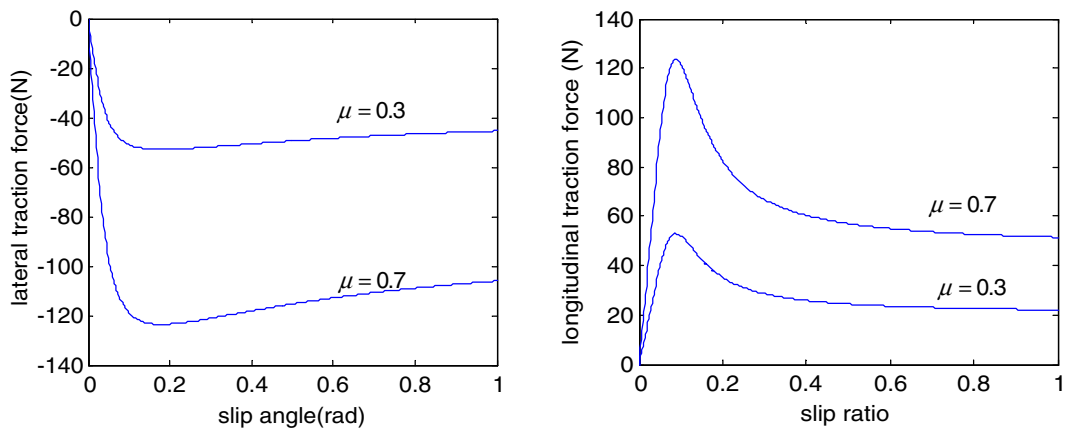

Fig. 2 **a** Lateral traction for friction coefficients 0.7 and 0.3. **b** Longitudinal traction for friction coefficients 0.7 and 0.3

3 Control Algorithms

3.1 Regulation Control

In the last section we observe that when both lateral and longitudinal slip dynamics are introduced into the WMR overall dynamic model, the overall WMR model becomes a third order under-actuated dynamic system with second order nonholonomic constraints. Such a model is different from a typical ideal WMR dynamic model in the sense that the second order nonholonomic constraint does not reduce the dimension of the state space. It has been shown that such a system is not asymptotically stabilizable to a given equilibrium solution using a time-invariant continuous feedback [15]. Therefore those control approaches for an ideal WMR dynamic model, such as backstepping technique in [24–26], and observer based controller in [27], cannot be applied to this model. However, such a system is asymptotically stabilizable to a desired equilibrium using time-invariant discontinuous feedback laws. A surface vessel is one such system where such time-invariant discontinuous feedback laws have been shown to work well. Surface vessel is modeled in local coordinates that are attached to the system. It is actuated in the surge and the yaw direction, while it is un-actuated in sway direction. In [15] a discontinuous coordinate transformation called σ-process is applied to transform an under-actuated surface vessel system into a discontinuous one in which the design of feedback control laws is carried out. Then, transforming back the system into the original coordinates yields discontinuous feedback laws that asymptotically stabilize the original system to the desired configuration with exponential convergence rate. In [28–30] the surface vessel model equations are transformed into a chained form where either discontinuous or time-varying feedback control laws can be designed to asymptotically drive the system to zero. In [31] a tracking control law is developed for an under-actuated surface vessel. Motivated by the above success, we develop a σ-process control technique for a WMR with wheel slip.

We transform the WMR dynamics in Eq. 1a into local coordinates that is attached to the WMR such that the un-actuated sidewise dynamics is explicit. We then apply the σ-process to transform the system into a discontinuous one, design a feedback control law and then transform back the system to the original coordinates to obtain a discontinuous controller.

In order to design this controller, we need to assume both slip ratio and slip angle are small and thus the traction force in Eq. 6 can be linearly approximated as follows [10],

$$F_3 = \beta \cdot sa \approx \beta \frac{\dot{\eta}}{v},\ F_i = \alpha \cdot sr_i = \alpha \frac{r\dot{\theta}_i - v_i}{v_i},\ i = 1, 2 \tag{8}$$

where $\alpha > 0$ and $\beta < 0$ are constants. Note that, in the turning control design in next section, linear approximation is not assumed and the nonlinearity of traction force is exploited to design the control.

In the pure rolling case, there is a mapping between v, $w(w = \dot{\varphi})$ and $\dot{\theta}_1, \dot{\theta}_2$ as,

$$\begin{bmatrix} v \\ w \end{bmatrix} = \begin{bmatrix} r/2 & r/2 \\ r/2/b & -r/2/b \end{bmatrix} \begin{bmatrix} \dot{\theta}_1 \\ \dot{\theta}_2 \end{bmatrix}, \tag{9}$$

so that $\dot{\theta}_1, \dot{\theta}_2$ can be controlled to get output v and w. However, when the pure rolling is relaxed and slip is introduced, this mapping is no longer valid. If we keep $\dot{\theta}_1, \dot{\theta}_2$ as control inputs to the WMR, the system model will consist of Eqs. 1a and 8. In the following steps, we design control inputs $\dot{\theta}_1, \dot{\theta}_2$.

The kinematic model of the WMR is

$$\begin{aligned} \begin{bmatrix} \dot{x}_0 \\ \dot{y}_0 \\ \dot{\varphi} \end{bmatrix} &= \begin{bmatrix} -\sin\varphi & \cos\varphi & 0 \\ \cos\varphi & \sin\varphi & 0 \\ 0 & 0 & 1 \end{bmatrix} \begin{bmatrix} \dot{\eta} \\ v \\ w \end{bmatrix} \\ &= \begin{bmatrix} -\sin\varphi & \cos\varphi & 0 \\ \cos\varphi & \sin\varphi & 0 \\ 0 & 0 & 1 \end{bmatrix} \begin{bmatrix} 1 & 0 & 0 \\ 0 & 1/2 & 1/2 \\ 0 & 1/2/b & -1/2/b \end{bmatrix} \\ &\quad \times \begin{bmatrix} \dot{\eta} \\ v_1 \\ v_2 \end{bmatrix} \end{aligned} \tag{10}$$

where x_0, y_0, φ denote the configuration of point P_0 in Fig. 1, and since $x_c = x_0 + d\cos\varphi$, $y_c = y_0 +$

$d \sin\varphi$, the dynamic model in Eq. 1a can be transformed into

$$\mathbf{M}\dot{\boldsymbol{\upsilon}} + \mathbf{C}(\dot{\varphi})\,\boldsymbol{\upsilon} = \mathbf{F}, \tag{11}$$

where, $\boldsymbol{\upsilon} = [\dot{\eta}\ \ v_1\ \ v_2]^T$, $\mathbf{F} = [F_3\ \ F_1\ \ F_2]$, $\mathbf{C} = \frac{m}{2}\dot{\varphi}\begin{bmatrix} 0 & 1 & 1 \\ -1 & 0 & 1 \\ -1 & -1 & 0 \end{bmatrix}$, $\mathbf{M}^{-1} = \begin{bmatrix} A & -b\,B & b\,B \\ -b\,B & E-b\,D & E+b\,D \\ b\,B & E+b\,D & E-b\,D \end{bmatrix}$. ($A$, B, D, E are nonzero constants (Appendix)).

When we define new state variables z_1, z_2, z_3, z_4, z_5, z_6 as

$$\begin{aligned} z_1 &= -x_0 \sin\varphi + y_0 \cos\varphi - \frac{b\,B}{D}\varphi \\ z_2 &= x_0 \cos\varphi + y_0 \sin\varphi \\ z_3 &= \varphi \\ [z_4, z_5, z_6]^T &= M\upsilon \end{aligned} \tag{12}$$

we will have a new set of equations as

$$\dot{z}_1 = \left(A + \frac{b\,BB}{D} + Bz_2\right) z_4 + Dz_2\,(z_5 - z_6) \tag{13}$$

$$\begin{aligned} \dot{z}_2 = &-B\left(z_1 + \frac{b\,B}{D} z_3\right) z_4 + (E - Dz_1 - b\,Bz_3)\,z_5 \\ &+ (E + Dz_1 + b\,Bz_3)\,z_6 \end{aligned} \tag{14}$$

$$\dot{z}_3 = -Bz_4 - Dz_5 + Dz_6 \tag{15}$$

$$\begin{aligned} \dot{z}_4 = &-(-Bz_4 - D\,(z_5 - z_6))\,mE\,(z_5 + z_6) \\ &+ \beta(Az_4 - b\,B\,(z_5 - z_6))\,(|-b\,Bz_4 + E(z_5 + z_6) \\ &- b\,D(z_5 - z_6)|^{-1} + |b\,Bz_4 + E(z_5 + z_6) \\ &+ b\,D(z_5 - z_6)|^{-1}) \end{aligned} \tag{16}$$

$$\dot{z}_5 = u_1 \tag{17}$$

$$\dot{z}_6 = u_2 \tag{18}$$

where

$$u_1 = \frac{1}{2} m\dot{\varphi}\,(\dot{\eta} - v_2) + \alpha \frac{r\dot{\theta}_1 - v_1}{v_1}, \tag{19}$$

$$u_2 = \frac{1}{2} m\dot{\varphi}\,(\dot{\eta} + v_1) + \alpha \frac{r\dot{\theta}_2 - v_2}{v_2} \tag{20}$$

As stated in [15], such a system cannot be exponentially stabilized at an equilibrium using smooth feedback, and it is not asymptotically stabilizable to a desired equilibrium solution using time-invariant continuous feedback. Define $\mathrm{z} = (\mathrm{z}_1, \mathrm{z}_2, \mathrm{z}_3, \mathrm{z}_4, \mathrm{z}_5, \mathrm{z}_6)^{\mathrm{T}} \in \mathbf{M}$, and the set of equilibrium manifold $\mathbf{M}^{\mathrm{e}} = \{\mathrm{z} \in \mathbf{M} | \mathrm{z}_4 = \mathrm{z}_5 = \mathrm{z}_6 = 0\}$, follow [15] and one can prove that the system described by Eqs. 13–18 is strongly accessible on $\mathbf{M}$, and it is small-time locally controllable at any equilibrium $\mathrm{z}^{\mathrm{e}} \in \mathbf{M}^{\mathrm{e}}$.

Now we design a time-invariant discontinuous feedback control law for the above system. We focus only on the problem of feedback stabilization to the origin, i.e., $\mathrm{z}^{\mathrm{e}} = 0$.

Stabilization of the Reduced System We first study the following reduced order system, which is obtained by considering the subsystem in Eqs. 13–16, letting ($\mathrm{z}_5 + \mathrm{z}_6$, $\mathrm{z}_5 - \mathrm{z}_6$) to be the control variables (v_1,v_2):

$$\dot{z}_1 = \left(A + \frac{b\,BB}{D} + Bz_2\right) z_4 + Dz_2\mathrm{v}_2 \tag{21}$$

$$\begin{aligned} \dot{z}_2 = &-B\left(z_1 + \frac{b\,Bz_3}{D}\right) z_4 + E\mathrm{v}_1 \\ &- D\left(z_1 + \frac{b\,Bz_3}{D}\right) \mathrm{v}_2 \end{aligned} \tag{22}$$

$$\dot{z}_3 = -Bz_4 - D\mathrm{v}_2 \tag{23}$$

$$\begin{aligned} \dot{z}_4 = &-\big(-Bz_4 - D\mathrm{v}_2\big) mE\mathrm{v}_1 + \beta\big(Az_4 - b\,B\mathrm{v}_2\big) \\ &\times \big(|-b\,Bz_4 + E\mathrm{v}_1 - b\,D\mathrm{v}_2|^{-1} \\ &+ |\,b\,Bz_4 + E\mathrm{v}_1 + b\,D\mathrm{v}_2\,|^{-1}\big) \end{aligned} \tag{24}$$

Consider the above reduced system in Eqs. 21–24. Restricting consideration to $z_3 \neq 0$, we apply the σ-process in [15]

$$y_1 = z_3,\ x_2 = z_2,\ x_3 = \frac{z_1}{z_3},\ x_4 = \frac{z_4}{z_3} \tag{25}$$

to obtain

$$\dot{y}_1 = -By_1x_4 - D\mathrm{v}_2 \tag{26}$$

$$\dot{x}_2 = E\mathrm{v}_1 - B\left(y_1x_3 + \frac{b\,By_1}{D}\right)y_1x_4 - D\left(y_1x_3 + \frac{b\,By_1}{D}\right)\mathrm{v}_2 \tag{27}$$

$$\dot{x}_3 = \left(A + \frac{b\,BB}{D} + Bx_2\right)x_4 + \frac{Dx_2\mathrm{v}_2}{y_1} + \frac{x_3}{y_1}\left(By_1x_4 + D\mathrm{v}_2\right) \tag{28}$$

$$\dot{x}_4 = -\frac{1}{y_1}\left(-By_1x_4 - D\mathrm{v}_2\right)mE\mathrm{v}_1 + \frac{\beta}{y_1}(Ay_1x_4 - b\,B\mathrm{v}_2) \times \left(|-b\,By_1x_4 + E\mathrm{v}_1 - b\,D\mathrm{v}_2|^{-1} + |b\,By_1x_4 + E\mathrm{v}_1 + b\,D\mathrm{v}_2|^{-1}\right) + \frac{x_4}{y_1}(By_1x_4 + D\mathrm{v}_2) \tag{29}$$

We design the feedback law to be

$$\mathrm{v}_1 = (-l_1x_2 - l_2x_3)/E, \tag{30}$$

$$\mathrm{v}_2 = (k_1y_1 - By_1x_4)/D, \tag{31}$$

where $k_1 > 0$ and l_1, l_2 are the gains, to derive the reduced closed loop system

$$\dot{y}_1 = -k_1y_1 \tag{32}$$

$$\dot{x}_2 = -l_1x_2 - l_2x_3 - k_1\left(x_3 + \frac{b\,B}{D}\right)y_1^2 \tag{33}$$

$$\dot{x}_3 = \left(A + \frac{b\,BB}{D}\right)x_4 + k_1x_2 + k_1x_3 \tag{34}$$

$$\dot{x}_4 = -k_1m\left(l_1x_2 + l_2x_3\right) + k_1x_4 + \beta\left(\left(A + \frac{b\,BB}{D}\right)x_4 - k_1\frac{b\,B}{D}\right) \times \left(|\gamma_1|^{-1} + |\gamma_2|^{-1}\right) \tag{35}$$

where $\gamma_1 = -l_1x_2 - l_2x_3 - k_1b\,y_1$ and $\gamma_2 = -l_1x_2 - l_2x_3 + k_1b\,y_1$.

The x-dynamics can be rewritten as

$$\dot{\mathbf{x}} = \left(\mathbf{A}_1 + \mathbf{A}_2(t)\right)\mathbf{x} + \mathbf{h}_1(t) \tag{36}$$

where

$$\mathbf{x} = \begin{bmatrix} x_2 & x_3 & x_4 \end{bmatrix}^T \tag{37}$$

$$\mathbf{A}_1 = \begin{bmatrix} -l_1 & -l_2 & 0 \\ k_1 & k_1 & A + \frac{b\,BB}{D} \\ -k_1l_1m & -k_1l_2m & k_1 + \beta\left(A + \frac{b\,BB}{D}\right)\left(|\gamma_1|^{-1} + |\gamma_2|^{-1}\right) \end{bmatrix}, \quad \mathbf{A}_2(t) = \begin{bmatrix} 0 & -k_1x_{10}^2e^{-2k_1t} & 0 \\ 0 & 0 & 0 \\ 0 & 0 & 0 \end{bmatrix}, \tag{38}$$

$$\mathbf{h}_1(t) = \left[-k_1\frac{b\,B}{D}y_{10}^2e^{-2k_1t},\ 0,\ -k_1\beta\frac{b\,B}{D}\left(|\gamma_1|^{-1} + |\gamma_2|^{-1}\right)\right]^T. \tag{39}$$

It can be seen that if $0 < l_1 < l_2$ and $k_1 + \beta\left(A + \frac{b\,BB}{D}\right)\left(|\gamma_1|^{-1} + |\gamma_2|^{-1}\right) < 0$, the eigenvalues of matrix A_1 can be assigned arbitrarily on the left-hand side of the phase plane. Note that $k_1 + \beta\left(A + \frac{b\,BB}{D}\right)\left(|\gamma_1|^{-1} + |\gamma_2|^{-1}\right) < 0$ can be satisfied when set an upper bound for the WMR's forward speed. Clearly, the y_1-dynamics is globally exponentially stable at $y_1 = 0$. Moreover, since matrix $\mathbf{A}_2(t)$ and $\mathbf{h}_1(t)$ go to zero as $t \to \infty$(note that $\left(|\gamma_1|^{-1} + |\gamma_2|^{-1}\right)$, representing the lateral traction term, will disappear when z_3 converges to zero), and

$$\int_0^\infty \|\mathbf{A}_2(t)\|\,dt < \infty, \int_0^\infty \|\mathbf{h}_1(t)\|\,dt < \infty,$$

the x dynamics can also be globally exponentially stable at the origin $x = 0$ when matrix $\mathbf{A}_1$ is a Hurwitz matrix [32].

Note that in the (z_1, z_2, z_3, z_4) coordinates the control law takes the form of

$$v_1(z_1, z_2, z_3, z_4) = \left(-l_1 z_2 - l_2 \frac{z_1}{z_3}\right)/E \tag{40}$$

$$v_2(z_1, z_2, z_3, z_4) = (k_1 z_3 - B z_4)/D \tag{41}$$

and the reduced closed-loop system becomes

$$\dot{z}_1 = \left(A + \frac{b\,B\,B}{D}\right) z_4 + k_1 z_2 z_3 \tag{42}$$

$$\dot{z}_2 = -l_1 z_2 - l_2 \frac{z_1}{z_3} - k_1 z_3 \left(z_1 + \frac{b\,B}{D} z_3\right) \tag{43}$$

$$\dot{z}_3 = -k_1 z_3 \tag{44}$$

$$\begin{aligned}\dot{z}_4 = {} & k_1 z_3 m \left(-l_1 z_2 - l_2 \frac{z_1}{z_3}\right) \\ & + \beta \left(\left(A + \frac{b\,B\,B}{D}\right) z_4 - k_1 \frac{b\,B}{D} z_3\right) \\ & \times \left(\left|-l_1 z_2 - l_2 \frac{z_1}{z_3} - k_1 b\, z_3\right|^{-1}\right. \\ & \left. + \left|-l_1 z_2 - l_2 \frac{z_1}{z_3} + k_1 b\, z_3\right|^{-1}\right)\end{aligned} \tag{45}$$

It can be shown that both the trajectory ($z_1(t)$, $z_2(t)$, $z_3(t)$, $z_4(t)$) and (v_1(t), v_2(t)) are bounded for all $t \geq 0$ and they converge exponentially to zero. Moreover, the control law in Eqs. 40 and 41 drives the system in Eqs. 42–45 to the origin, while avoiding the set

$$\mathbf{N} = \{(z_1, z_2, z_3, z_4) \,|z_3 = 0, (z_1, z_2, z_4) \neq 0\}.$$

Stabilization of the Complete System Now we study the problem of asymptotic stabilization of the complete system in Eqs. 13–18, with u_1 and u_2, instead of z_5 and z_6, as control inputs. However, the integrator back-stepping approach developed for smooth systems cannot be directly applied here to derive control inputs due to the discontinuous nature of the system.

Consider the controllers satisfying the following equations:

$$\begin{aligned}u_1(z) + u_2(z) = {} & -K(z_5 + z_6 - v_1(z_1, z_2, z_3, z_4)) \\ & + s_1(z)\end{aligned} \tag{46}$$

$$\begin{aligned}u_1(z) - u_2(z) = {} & -L(z_5 - z_6 - v_2(z_1, z_2, z_3, z_4)) \\ & + s_2(z)\end{aligned} \tag{47}$$

where v_1 and v_2 are feedback laws for reduced system, and s_1 and s_2 correspond to their time derivatives along Eqs. 13–18

$$\begin{aligned}s_1(z) = {} & \frac{1}{E}\left(l_1\left(-B\left(z_1 + \frac{b\,B}{D} z_3\right) z_4 + E(z_5 + z_6)\right.\right. \\ & \left. - (D z_1 + b\,B z_3)(z_5 - z_6)\right) \\ & + \frac{l_2}{z_3}\left(\left(A + \frac{b\,B\,B}{D} + B z_2\right) z_4\right. \\ & \left. + D z_2 (z_5 + z_6)\right) \\ & \left. + l_2 \frac{z_1}{z_3}(B z_4 + D(z_5 - z_6))\right)\end{aligned}$$

$$\begin{aligned}s_2(z) = {} & \frac{1}{D}\big(-k_1(B z_4 + D(z_5 - z_6)) \\ & + B(B z_4 + D(z_5 - z_6)) m E(z_5 + z_6) \\ & - B\beta(A z_4 - b\,B(z_5 - z_6)) \\ & \times \big(|-b\,B z_4 + E(z_5 + z_6) - b\,D(z_5 - z_6)|^{-1} \\ & + |b\,B z_4 + E(z_5 + z_6) + b\,D(z_5 - z_6)|^{-1}\big)\big)\end{aligned}$$

The idea is to implement the control law in Eqs. 40 and 41 through the integrators by choosing gains K and L appropriately.

Consider the coordinate transformation

$$y_1 = z_3, x_2 = z_2, x_3 = \frac{z_1}{z_3}, x_4 = \frac{z_4}{z_3},$$

$$w_1 = z_5 + z_6 + \left(l_1 z_2 + l_2 \frac{z_1}{z_3}\right)/E,$$

$$w_2 = z_5 - z_6 - (k_1 z_3 - B z_4)/D$$

Then, it can be shown that the close-loop system can be written as

$$\dot{y}_1 = -k_1 y_1 - D w_2 \tag{48}$$

$$\dot{\mathbf{x}} = \left(\mathbf{A}_1 + \tilde{\mathbf{A}}_2(t)\right)\mathbf{x} + \mathbf{h}_2(t) \tag{49}$$

$$\dot{w}_1 = -K w_1 \tag{50}$$

$$\dot{w}_2 = -L w_2 \tag{51}$$

where $\mathbf{A}_1$ is the matrix given by Eq. 37 and

$$\tilde{\mathbf{A}}_2(t) = \begin{bmatrix} 0 & r_1(t) & 0 \\ r_2(t) & r_2(t) & 0 \\ -l_1 m r_2(t) & -l_2 m r_2(t) & r_2(t) \end{bmatrix}$$

$$r_1(t) = -\left(y_{10}e^{-k_1 t} + \frac{E w_{20}}{L - k_1}e^{-Lt}\right) \times \left(k_1 y_{10}e^{-k_1 t} + \frac{L D w_{20}}{L - k_1}e^{-Lt}\right)$$

$$r_2(t) = D\left(y_{10}e^{-k_1 t} + \frac{D w_{20}}{L - k_1}e^{-Lt}\right)^{-1} w_{20}e^{-Lt}$$

$$\mathbf{h}_2(t) = \Bigg[-k_1\frac{b\,B}{D}y_{10}^2 e^{-2k_1 t} - b\,B y_{10} w_{20} e^{-(L+k_1)t} + E w_{10}e^{-Kt},\ 0,\ m E w_{10}e^{-Kt}(k_1 + r_2(t)) - \beta\frac{b\,B}{D}(k_1 + r_2(t))\left(\frac{1}{|\gamma_1'|} + \frac{1}{|\gamma_2'|}\right)\Bigg]^T$$

where $\gamma_1' = l_1 x_2 - l_2 x_3 - k_1 b\, x_1 + E w_{10}e^{-Kt} - b D w_{20}e^{-Lt}$ and $\gamma_2' = k_1 b x_1 - l_1 x_2 - l_2 x_3 + E w_{10}e^{-Kt} + b\, D w_{20}e^{-Lt}$.

The (y_1, w_1, w_2)-dynamics is globally exponentially stable at $(y_1, w_1, w_2) = (0, 0, 0)$. It can be shown that if $K > k_1$ and $y_{10}w_{10} \geq 0$ (i.e. $z_{30}(z_{50} + z_{60} + l_1 z_{20}/E) + l_2 z_{10}/E \geq 0$) then $\tilde{\mathbf{A}}_2(t)$ and $\mathbf{h}_2(t)$ go to zero as $t \to \infty$ and

$$\int_0^\infty \left\|\tilde{\mathbf{A}}_2(t)\right\| dt < \infty, \int_0^\infty \|\mathbf{h}_2(t)\|\, dt < \infty.$$

Thus, for any initial condition $(y_{10}, x_0, w_{10}, w_{20})$ satisfying $y_{10} \neq 0$ and $y_{10}w_{10} \geq 0$, both the trajectory $(y_1(t), x(t), w_1(t), w_2(t))$ and the control $(u_1(t), u_2(t))$ are bounded for all $t \geq 0$ and converge exponentially to zero. Furthermore, the trajectory $(z_1(t), z_2(t), z_3(t), z_4(t), z_5(t), z_6(t))$ is bounded for all $t \geq 0$ and converges exponentially to zero.

3.2 Turning Control

In an ABS control system of a vehicle, wheel slip has been controlled via sliding mode to maintain the longitudinal traction force at its maximum [16], such that the vehicle can stop with highest possible deceleration. In this paper we apply sliding mode to control a WMR to drive its lateral traction force to its maximum and maintain it during turning, such that the WMR can make a sharpest possible turn. If the optimal wheel slip is known, where the traction force is maximal, slip can be controlled directly to maintain at its optimal value. However, when both the optimal lateral slip speed and the analytic form of the lateral traction force are unknown, we apply a sliding mode-based extremum seeking control (ESC) technique such that the WMR conducts turning with maximum lateral traction force, which gives a minimum allowed radius of curvature for a given forward speed [33]. In addition, the longitudinal traction force is estimated via a sliding mode-based observer in [16] using the information of angular speeds of the wheels. In this paper, we design a sliding mode based observer to estimate the lateral traction force that will be used in the ESC design, using the information of angular speeds of both the robot and the wheels.

Since the WMR is not actuated in the lateral direction, the lateral traction force is controlled indirectly by controlling the longitudinal traction forces for the two wheels, and the longitudinal traction forces are controlled by the wheel torques. In the following section we design longitudinal traction forces both to control the lateral traction force towards its maximum and to control the forward speed. The input torques are then designed via standard sliding mode to control the longitudinal traction forces, which is omitted in this paper.

3.2.1 Optimum Search Algorithm for Lateral Traction

Differentiating the lateral traction F_3 with respect to time along the trajectories of the system (1)–(5) we obtain

$$\frac{dF_3}{dt} = \frac{\partial F_3}{\partial (sa)} \frac{1}{v^2 + \dot{\eta}^2} \times \left[-\frac{db\, v}{I} (F_1 - F_2) - \frac{\dot{\eta}}{m} (F_1 + F_2) + F_3 \left(\frac{v}{m} + \frac{d^2 v}{I} \right) - \dot{\varphi} \left(v^2 + \dot{\eta}^2 + d\dot{\varphi}\dot{\eta} \right) \right] + \frac{\partial F_3}{\partial t} \tag{52}$$

Define an error variable $e = F_3 - F_3^r$ where F_3^r is an upper bound of F_3. Then the dynamics for e is governed by

$$\frac{de}{dt} = \frac{\partial F_3}{\partial (sa)} \frac{v}{v^2 + \dot{\eta}^2} \left[A(\dot{\eta}, \dot{\varphi}, v, F_1, F_2) + Bu_1 \right] + \frac{\partial F_3}{\partial t} \tag{53}$$

where

$$A(\dot{\eta}, \dot{\varphi}, v, F_1, F_2) = -\frac{\dot{\eta}}{mv} (F_1 + F_2) + F_3 \left(\frac{1}{m} + \frac{d^2}{I} \right) - \dot{\varphi} \left(v^2 + \dot{\eta}^2 + d\dot{\varphi}\dot{\eta} \right) / v, \tag{54}$$

$$B = -\frac{db}{I}, \tag{55}$$

and u_1 is the new control input defined as $u_1 = F_1 - F_2$.

We design the sliding surface as

$$s = e + \int_0^t \lambda e d\tau, \tag{56}$$

where $\lambda > 0$. If s converges to a constant, the sliding motion satisfies

$$\frac{de}{dt} + \lambda e \to 0, \tag{57}$$

and the lateral traction force can be made to its maximum with a proper selection of λ. To obtain the control law to let s converge to a constant, first we rewrite Eq. 56 together with Eq. 53 as

$$\frac{ds}{dt} = \frac{\partial F_3}{\partial (sa)} \frac{v}{v^2 + \dot{\eta}^2} \left[A(\dot{\eta}, \dot{\varphi}, v, F_1, F_2) + Bu_1 \right] + \frac{\partial F_3}{\partial t} + \lambda e. \tag{58}$$

Let $A = \overline{A} + \Delta A$ where $\overline{A}$ represent the nominal part of A whereas the unknown part ΔA is bounded by $|\Delta A| \leq \delta A$. Design the control law as

$$u_1 = -B^{-1} \left(\overline{A} + \gamma \Phi(s) \right), \tag{59}$$

where $\gamma = \delta A + N$ with $N > 0$, and $\Phi(s) = \operatorname{sgn} \sin(2\pi s/\alpha)$, a periodic switching function [16, 34], which periodically search the traction force neighborhood to determine the control direction. This selection guarantees that s converges to $k\alpha$ for some integer k, which depends on the initial condition and F_3^r, if the following sliding mode existence condition is satisfied:

$$\left| \frac{\partial F_3}{\partial (sa)} \frac{v}{v^2 + \dot{\eta}^2} (\delta A + N) \right| > \left| \frac{\partial F_3}{\partial (sa)} \frac{v}{v^2 + \dot{\eta}^2} \Delta A + \frac{\partial F_3}{\partial t} + \lambda e \right|. \tag{60}$$

If it is assumed that the explicit dependence of traction on time is negligible, and keep in mind that $|\Delta A| \leq \delta A$, the sliding mode existence condition turns into

$$\left| \frac{\partial F_3}{\partial (sa)} \right| \frac{v}{v^2 + \dot{\eta}^2} N > \lambda |e|. \tag{61}$$

Thus in sliding mode, the lateral traction force will converge to F_3^r until it enters a region where the gradient is so small that the condition (60) cannot be satisfied. When Eq. 60 is not satisfied, the traction is close to its maximum and it will behave arbitrarily. However, for a given F_3^r and λ, we can select a sufficiently large N such that this region around the maximum can be made arbitrarily small. In future simulations we select $\lambda = 0.5$ and $\alpha = 0.5$.

3.2.2 Forward Speed Control

From Eqs. 1–5 we know that the forward speed is governed by

$$m\dot{v} = F_1 + F_2 + m\dot{\varphi}\left(\dot{\eta} + d\dot{\varphi}\right), \tag{62}$$

which we rewrite as

$$m\dot{v} = u_2 + m\dot{\varphi}\left(\dot{\eta} + d\dot{\varphi}\right), \tag{63}$$

where u_2 is the new control input defined as $u_2 = F_1 + F_2$.

We design sliding surface as

$$s = v - v_r, \tag{64}$$

where v_r is the desired speed. If s converges to zero, v will converge to v_r. The sliding surface is governed by

$$\dot{s} = \frac{u_2}{m} + \dot{\varphi}\left(\dot{\eta} + d\dot{\varphi}\right) = \frac{u_2}{m} + C\left(\dot{\varphi}, \dot{\eta}\right). \tag{65}$$

Let $C = \overline{C} + \Delta C$ where $\overline{C}$ represents the nominal part of C whereas the unknown part ΔC is bounded by $|\Delta C| \leq \delta C$.

Design the control law as

$$u_2 = -m\overline{C} + mk\ \mathrm{sgn}(s), \tag{66}$$

where $k = \delta C + \mu$ with $\mu > 0$, such that s converges to zero.

3.2.3 Lateral Traction Observer

The realization of the ESC algorithm requires the knowledge of the lateral traction force. We assume this quantity cannot be measured directly, so we develop an observer that allows us to obtain lateral traction force using the measurements of the robot angular speed $\dot{\varphi}$ and the wheel angular speed $\dot{\theta}_i$. This observer is based on the equivalent control method, which has been used to develop observer for longitudinal traction force in ABS control in [16].

From Eq. 1 we derive the dynamic equation

$$Ir\ddot{\varphi} + I_w b\left(\ddot{\theta}_1 - \ddot{\theta}_2\right) = (\tau_1 - \tau_2)b - F_3 rd. \tag{67}$$

Now we define a new variable $\zeta = \dot{\varphi} + \frac{I_w b}{Ir}\left(\dot{\theta}_1 - \dot{\theta}_2\right)$, which turns Eq. 67 into

$$Ir\dot{\zeta} = (\tau_1 - \tau_2)b - F_3 rd. \tag{68}$$

We define an estimate $\hat{\zeta}$ which satisfies

$$Ir\dot{\hat{\zeta}} = (\tau_1 - \tau_2)\, b - Vrd. \tag{69}$$

The function V is picked as

$$V = -N\ \mathrm{sgn}\left(\overline{\zeta}\right) \tag{70}$$

where $\overline{\zeta} = \zeta - \hat{\zeta}$ is a tracking error of ζ and $N > 0$ is a sufficiently large constant.

Subtracting Eq. 69 from Eq. 68 we obtain

$$Ir\dot{\overline{\zeta}} = -rdN\ \mathrm{sgn}(\overline{\zeta}) - rdF_3. \tag{71}$$

If N is selected such that $N > \max\{|F_3|\}$, $\overline{\zeta}$ converges to the sliding surface $\overline{\zeta} = 0$. On sliding surface the equivalent value of variable $V = -N\ \mathrm{sgn}\left(\overline{\zeta}\right)$ is equal to F_3

$$V_{eq} = F_3. \tag{72}$$

As shown in [16], the equivalent value of the high frequency switching signal can be obtained by applying a low pass filter

$$H(s) = \frac{1}{T_f s + 1}, \tag{73}$$

where T_f is the constant which suppresses the high frequency signal. Since this chattering only occurs in the lateral traction force observer loop, it will not affect the entire system. The estimate of the lateral traction force out of the filter will be used in the ESC algorithm.

3.2.4 Longitudinal Traction Force Tracking

From previous sections A and B, we obtain desired F_1 and F_2 to control lateral traction force and forward speed. Next, we can design τ_i to enable F_i to track desired F_i using sliding mode control, which is omitted in this paper.

4 Simulation Results

4.1 Regulation Control Simulation

We present simulation results to validate our discontinuous controller on the WMR model that include slip dynamics. For the simulation task, the WMR parameters (refer to Fig. 1) are as follows: $b = 0.24$ m; $d = 0.05$ m; $r = 0.095$ m; $m = 17$ kg; $I_{rz} = 0.537$; $I_{wy} = 0.0023$ kgm^2; $I_{wz} = 0.0011$ kgm^2. We apply our proposed controller to the stabilization problem that is subject to both lateral and longitudinal slips. The traction curve slope parameters are $\alpha = 20, \beta = -12$.

We set the origin as the desired configuration and simulate the problem with the initial position of the WMR $[x_0, y_0, \varphi_0] = [-2, -1, \pi/2]$, initial forward speed $\upsilon_0 = 0$ and initial angular speed $\omega_0 = 0$. The control gains are selected as : $K = 0.5$, $L = 0.5, k_1 = 0.044, l_1 = 1, l_2 = 2$.

In Fig. 3 we observe that the WMR trajectory converges to the origin. Figure 4 is the WMR configuration, where we observe that the WMR is able to converge to the origin with monotonically decreasing φ. The lateral and longitudinal slip speeds are shown in Figs. 5 and 6. It can be seen that the left side wheel needs more slip to generate more traction than the right wheel for the WMR to make a right turn. Figure 7 shows the control inputs $\dot{\theta}_1$ and $\dot{\theta}_2$, respectively. We observe that

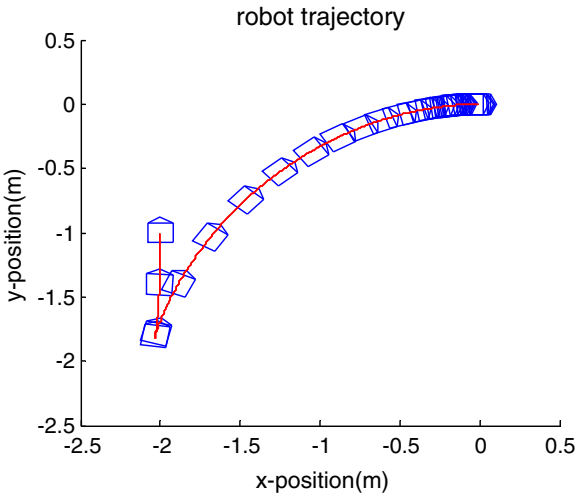

Fig. 3 WMR trajectory

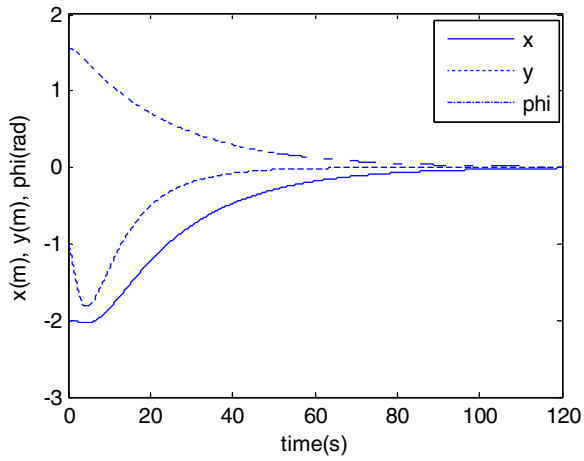

Fig. 4 WMR configuration

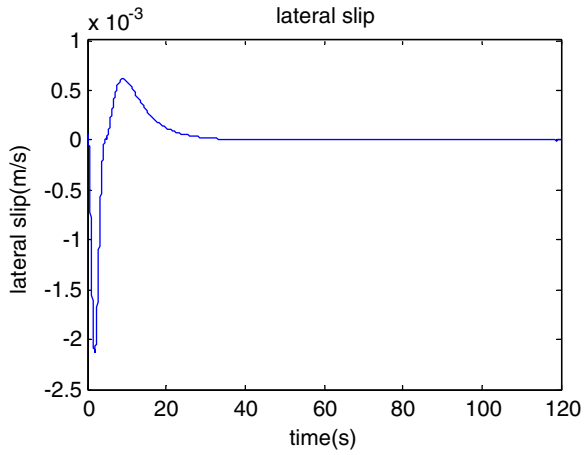

Fig. 5 Lateral slip speed

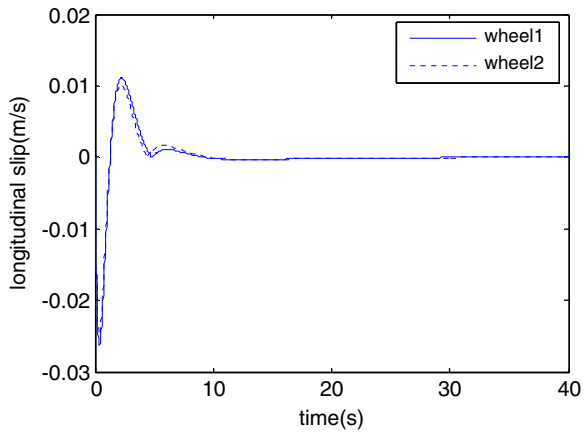

Fig. 6 Longitudinal slip speed for both wheels

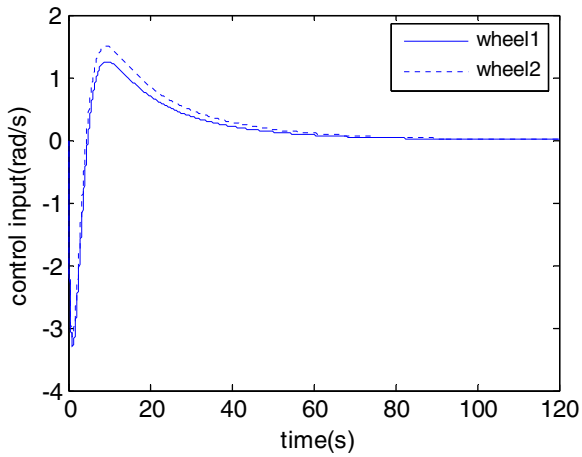

Fig. 7 Control inputs for wheel1 and wheel2

both the control inputs are bounded and converge to zero asymptotically.

4.2 Turning Control Simulation

Applying the sliding mode technique in Section 3, we show turning control simulation results in this section. Let the WMR start from the configuration [0,0,0] with initial and desired speed 2 m/s. The friction coefficient is 0.3. The sliding mode control law controls the robot to make a turn at almost constant curvature in Fig. 8. Figure 9 shows the lateral slip speed that stays close to optimal slip value where maximum traction force occurs. In Fig. 10 we observe that the actual lateral traction force oscillate closely to the maximum value indicated in Fig. 2. The estimated lateral traction force from the observer tracks the actual force nicely.

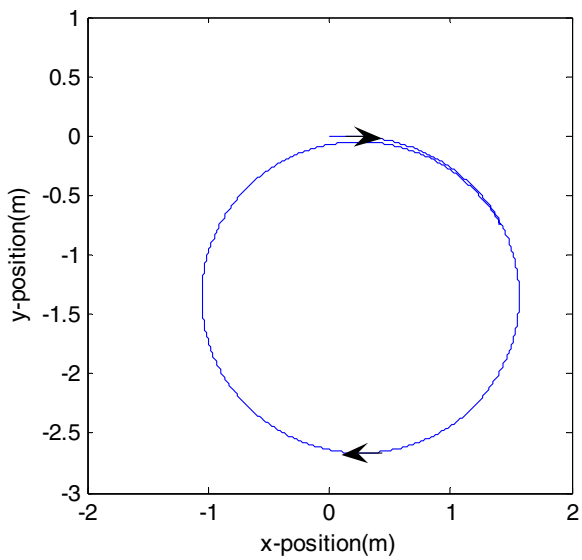

Fig. 8 Turning control trajectory

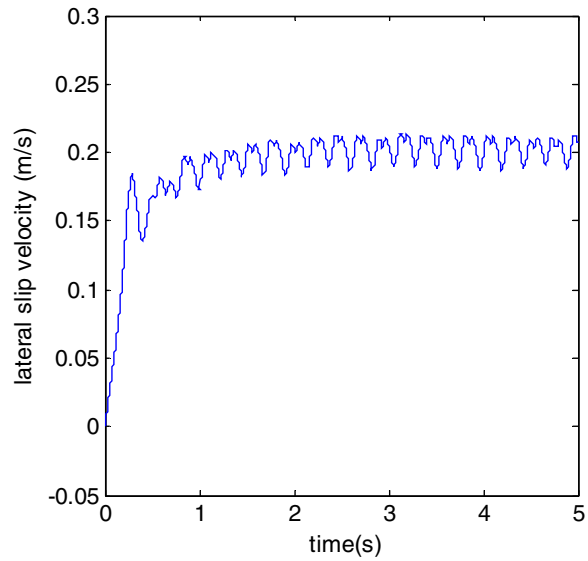

Fig. 9 Lateral slip speed in turning control

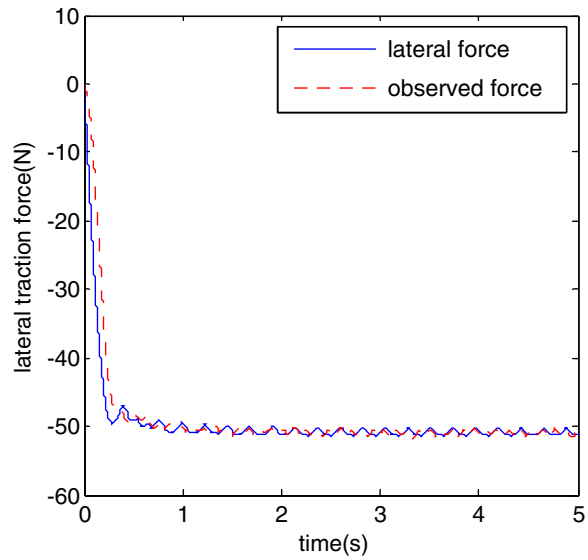

Fig. 10 Actual and observed lateral traction force

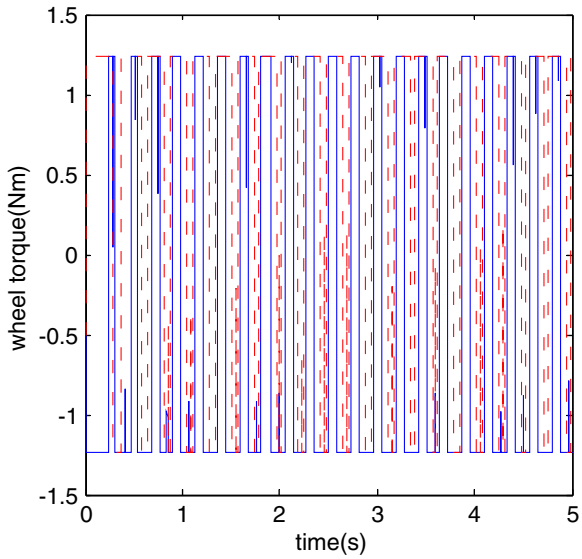

Fig. 11 Wheel torques

Figure 11 shows the wheel torque that generates switching control input for the WMR.

5 Conclusions

In this paper, we model the overall dynamics of a WMR subject to wheel slips. With slip dynamics incorporated into the model, the WMR becomes an under-actuated system. We propose a discontinuous control based on σ-process technique for regulation control task such that all three DOFs can be regulated. We then propose a sliding mode control based on extremum seeking control technique for sharp turning control task such that the lateral traction force can be maximized and the turning radius can be minimized. Simulations are conducted to verify the theoretical results. We believe that these new controllers will endow a WMR with the ability to maneuver on a slippery surface. Currently we could not perform an experiment to verify these controllers since we do not possess the ability to measure slip in real-time. However, as discussed earlier, several researchers are working in the area of real-time slip measurement [18–20] and we believe that such sensors will become standard in the WMRs of the future. Our current effort in designing controllers that can accommodate slip underscores the need for the development of such sensors.

Appendix

$$M=\begin{bmatrix} m & \frac{dm}{2b} & -\frac{dm}{2b} \\ \frac{dm}{2b} & \frac{I+m\left(d^2+b^2\right)}{4b^2} & -\frac{I+m\left(d^2-b^2\right)}{4b^2} \\ -\frac{dm}{2b} & -\frac{I+m\left(d^2-b^2\right)}{4b^2} & \frac{I+m\left(d^2+b^2\right)}{4b^2} \end{bmatrix}$$

$$M^{-1}=\begin{bmatrix} A & -b\,B & b\,B \\ -b\,B & E-b\,D & E+b\,D \\ b\,B & E+b\,D & E-b\,D \end{bmatrix}$$

$$=\begin{bmatrix} \frac{md^2+I}{mI} & -\frac{db}{I} & \frac{db}{I} \\ -\frac{db}{I} & \frac{mb^2+I}{mI} & -\frac{mb^2-I}{mI} \\ \frac{db}{I} & -\frac{mb^2-I}{mI} & \frac{mb^2+I}{mI} \end{bmatrix}$$

where $A=\frac{md^2+I}{mI}$, $B=\frac{d}{I}$, $D=-\frac{b}{I}$, $E=\frac{1}{m}$.

References

1. Motte, I., Campion, I.: A slow manifold approach for the control of mobile robots not satisfying the kinematic constraints. IEEE Trans. Robot. Autom. **16**(6), 875–880 (2000)
2. Lin, W.-S., Chang, L.-H., Yang, P.-C.: Adaptive critic anti-slip control of wheeled autonomous robot. Control Theory Appl. IET. **1**(1), 51–57 (2007)
3. Tarokh, M., McDermott, G.J.: Kinematics modeling and analyses of articulated rover. IEEE Trans. Robot. **21**(4), 539–553 (2005)
4. Dixon, W.E., Dawson, D.M., Zergeroglu, E.: Robust control of a mobile robot system with kinematic disturbance. In: IEEE Int. Conference on Control Applications, pp. 437–442 (2000)
5. Zhang, Y., Chung, J.H., Velinsky, S.A.: Variable structure control of a differentially steered wheeled mobile robot. J. Intell. Robot. Syst. **36**(3), 301–314 (2003)
6. Michalek, M.M., Dutkiewicz, P., Kielczewski, M., Pazderski, D.: Vector-field-orientation tracking control for a mobile vehicle disturbed by the skid-slip phenomena. J. Intell. Robot. Syst. **59**(304), 341–365 (2010)

7. Balakrishna, R., Ghosal, A.: Modeling of slip for wheeled mobile robot. IEEE Trans. Robot. Autom. **11**(1), 126–132 (1995)
8. Jung, S., Hsia, T.C.: Explicit lateral force control of an autonomous mobile robot with slip. In: IEEE/RSJ Int. Conf. on Intelligent Robots and Systems, IROS, pp. 388–393 (2005)
9. Stonier, D., Se, H.C., Sung-Lok, C., Kuppuswamy, N.S., Jong-Hwan, K.: Nonlinear slip dynamics for an omni-wheel mobile robot platform. In: IEEE Int. Conf. on Robotics and Automation, pp. 2367–2372 (2007)
10. Ploeg, J., Schouten, H.E., Nijmeijer, H.: Control design for a mobile robot including tire behavior. In: 2008 IEEE Intelligent Vehicles Symposium, pp. 240–245. Eindhoven, The Netherlands, 4–6 June 2008
11. Lagerberg, A., Egardt, B.: Backlash estimation with application to automotive powertrains. IEEE Trans. Control Syst. Technol. **15**(3), 483–493 (2007)
12. Verma, R., Vecchio, D., Fathy, H.: Development of a scaled vehicle with longitudinal dynamics of an HMMWV for an ITS testbed. IEEE/ASME Trans. Mechatron. **13**(1), 46–57 (2008)
13. Kyung-Ho, B.: Development of dynamics modeling in the vehicle simulator for road safety analysis. In: Annual Conference SICE07, pp. 649–653 (2007)
14. Der-Chen, L., Wen-Ching, C.: Control design for vehicle's lateral dynamics. In: IEEE Int. Conf. on Systems, Man and Cybernetics, ICSMC '06, vol. 3, pp. 2081–2086 (2006)
15. Reyhanoglu, M.: Exponential stabilization of an underactuated autonomous surface vessel. Automatica **33**(12), 2249–2254 (1997)
16. Drakunov, S., Ozguner, U., Dix, P., Ashrafi, B.: ABS control using optimum search via sliding modes. IEEE Trans. Control Syst. Technol. **3**(1), 79–85 (1995)
17. Sidek, N.: Dynamic modeling and control of nonholonomic wheeled mobile robot subjected to wheel slip. Ph.D. thesis, Vanderbilt University, USA (2008)
18. Ward, C.C., Iagnemma, K.: Model-based wheel slip detection for outdoor mobile robots. In: IEEE Int. Conf. on Robotics and Automation, pp. 2724–2729 (2007)
19. Angelova, A., Matthies, L., Helmick, D.M., Sibley, G., Perona, P.: Learning to predict slip for ground robots. In: Proc. of IEEE Int. Conf. on Robotics and Automation, pp. 3324–3331 (2006)
20. Seyr, M., Jakubek S.: Proprioceptive navigation, slip estimation and slip control for autonomous wheeled mobile robot. In: IEEE Conf. on Robotics, Automation and Mechatronics, pp. 1–6 (2006)
21. Germann, M., Wurtenberger, A., Daiss, A.: Monitoring of the friction coefficient between tyre and road surface. In: Proc. of the Third IEEE Conf. on Control Applications, pp. 613–618, 1 Aug 1994
22. Li, L., Wang, F.Y.: Integrated longitudinal and lateral tire/road friction modeling and monitoring for vehicle motion control. IEEE Trans. Intell. Transp. Syst. **7**(1), 1–9 (2006)
23. Bakker, E., Nyborg, L., Pacejka, H.B.: Tire modeling for the use of the vehicle dynamics studies. SAE paper 870421 (1987)
24. Fierro, R., Lewis, F.L.: Control of a nonholonomic mobile robot: backstepping kinematics into dynamics. J. Robot. Syst. **14**(3), 149–163 (1997)
25. Fukao, T., Nakagawa, H., Adachi, N.: Adaptive tracking control of a nnholonomic mobile robot. IEEE Trans. Robot. Autom. **16**(5), 609–615 (2000)
26. Jiang, Z.-P., Nijmeijer, H.: Tracking control of mobile robots: a case study in backstepping. Automatica **33**(7), 1393–1399 (1997)
27. Do, K.D., Jiang, Z.-P., Pan, J.: A global output-feedback controller for simultaneous tracking and stabilization of unicycle-type mobile robots. IEEE Trans. Robot. Autom. **20**(3), 589–594 (2004)
28. Mazenc, F., Pettersen, K., Nijmeijer, H.: Global uniform asymptotic stabilization of an underactuated surface vessel. IEEE Trans. Autom. Control. **47**(10), 1759–1762 (2002)
29. Dong, W., Guo, Y.: Global time-varying stabilization of underactuated surface vessel. IEEE Trans. Autom. Control **50**(6), 859–864 (2005)
30. Ghommam, J., Mnif, F., Benali, A., Derbel, N.: Asymptotic backstepping stabilization of an underactuated surface vessel. IEEE Trans. Control Syst. Technol. **14**(6), 1150–1157 (2006)
31. Behal, A., Dawson, D.M., Dixon, W.E., Fang, Y.: Tracking and regulation control of an underactuated surface vessel with nonintegrable dynamics. IEEE Trans. Autom. Control. **47**(3), 495–500 (2002)
32. Slotine, J.-J.E., Li, W.: Applied Nonlinear Control. Prentice-Hall, Englewood Cliffs, NJ (1991)
33. Tian, Y., Sarkar, N.: Near-optimal autonomous pursuit evasion for nonholonomic wheeled mobile robot subject to wheel slip. In: IEEE International Conference on Robotics and Automation, pp. 4946–4951. Anchorage, USA (2010)
34. Yu, H., Ozguner, U.: Extremum-seeking control stragegy for ABS system with time delay. Proc. Am. Control Conf. **5**, 3753–3758 (2002)